MIT
Center for Space Research   Chandra X-Ray Center

MEMORANDUM
July 20, 2004

To:	Dale Graessle, CALDB lead
From:	Bish K. Ishibashi, SDS
Subject:	Evaluation on the quality of LETG/ACIS-S LSFPARM file for unrandomized event datasets
Revision:	1.0
URL:	http://space.mit.edu/CXC/docs/memo_lsf_la_1.0.ps
File:	/nfs/cxc/h2/bish/CXC SDS/LSFDIR/HO_LSF_LA/memo_lsf_la_1.0.tex

1 Unrandomized LSFPARM files for LETG/ACIS-S Configuration

In Repro *III*, decisions have been made to turn off data randomization on TG R/D. This action necessitates rapid development of line spread function parameter files (LSFPARM) without built-in data randomization. By applying the similar LSF processing scheme[1], new LSFPARM files for LETG+ACIS-S configuration have been developed. This document describes the quality of the new LSFPARM products.

2 Building LSFPARM

Procedures for building a LSFPARM file is described at:

http://space.mit.edu/CXC/LSFX/LSF_valid2.html

For rapid development, several parts of IDL parameterization routines are S-Langified for better and faster convergence to optimum fitting parameters through automated processes.

3 Data products

Two LSFPARM products are developed: LEG $\pm$ 1^{st} orders configuration with LETG+ACIS-S without data randomization in TG coordinate. Evaluation of the two products are documented in the following section. The existing LSF product for LETG+ACIS-S configuration in CALDB contains LSFPARM with only one extraction width, hence limiting the way any LETG+ACIS-S dataset is reprocessed for analysis. The new products, on the other hand, contain ten different extraction widths, hence making it more versatile for custom extraction by users.

[1] See an example in https://icxc.harvard.edu/calco/ard_updates/ECR/Approved_ECRs/ECR_2002_016.html

Table 1. New header keywords for LSFPARM

Keyword	Value	Comment
RAND_TG	0.0	No data randomization in TG values
CBD60001	RAND_TG(0.0)	CALDB query expression

3.1 Header Keyword for Data Randomization

Two new FITS header keywords – RAND_TG and CBD60001 – are included in each LSFPARM product in order to specify whether LSFPARM products is for randomized datasets or not. For a unrandomized dataset, these header keywords are set to the values as listed in Table 1. These keywords would enable to form proper CALDB query expression and to search for unrandomized LSFPARM products.

4 Testing LSFPARM products

4.1 Procedures

Testing of the LSFPARM products are performed with MARX simulated and real Capella (ObsID 55) datasets. Two key points of our interests are (1) line profile and (2) encircled energy fractions (hereafter EEFRAC).

4.2 Evaluation I. MARX-Simulated Dataset

Mono-energetic beam simulations are performed with MARX at various energy values and concatenated together to make a L1 event file. The L1 file has gone through nominal CIAO 3.1 processing, except that pixel randomization in TG space being turned off at *tg_resolve_events*. Corresponding grating RMF files are generated via *mkgrmf* command with the new LSFPARM files and used as a fitting kernel in *ISIS* for evaluation. Cash statistics is applied throughout this work.

4.2.1 Line Profile Analysis

If the LSFPARM products are valid, simulated line profiles can be described with a Kronecker delta function folded over grating RMFs. Figures 1 and 2 show several line profiles fitted with a delta function. For brevity, selected six of 12 line samples are shown in each figure for inspection: lines at E = 200, 275, 450, 800, 1100, and 2000 eV. These are representative of the results of other line profile fittings, resulting in the value of goodness of fit generally less than 1.8 for LEG (these are not meant to be necessarily the best fitting results).

Despite modestly high S/N ratio in these line profile simulations, the model fitting has resulted in the reasonable χ^2 values in Cash statistic; hence the results validate that the LSF parameterization are completed just as well as with the HETG configuration system done earlier.

4.2.2 Encircled Energy Fraction

The second key component of LSFPARM products is the value of encircled energy fraction as a function of energy. The value EEFRAC is derived from cross-dispersion line profile of a mono-energetic beam, integrated over arbitrary extraction width centered around the line peak (or in Chandra's term, at TG_D = 0 degree). If derived correctly, EEFRAC will allow users to correct measured count rates (or fluxes) for an aperture size per extraction.

The following tests are performed such that the simulated line spectra (samples shown in Figures 1 and 2) are extracted at three different aperture sizes; then the delta-function model is fitted to 12 mono-energetic lines in order to derive model line fluxes F_m in counts s^{-1}. ISIS is also enabled to provide cumulative counts in each line, which is used to derive a "observed" line flux F_d. In an ideal condition, both the model and observed line fluxes should be identical, i.e.,

$$\frac{F_d}{F_m} \approx 1.$$

Two LEG configurations (LEG $\pm$ 1st) are tested and verified that the new LSFPARM products meet this criterion within a few percentage (see Tables 2 and 3), presumably better than our knowledge in effective area of Chandra's HRMA system.

4.3 Remark on Evaluation I.

The part I of the evaluation concludes that the new LSFPARM products are good representation of the LETG+ACIS-S calibration benchmark that the current MARX provides. Note that MARX incorporates the collective knowledges that are provided via the Chandra calibration group.

4.4 Evaluation II. Chandra Dataset

The same two LSFPARM products are tested against real Chandra observation (Capella, ObsID = 55) in the similar manner as performed on the simulated datasets.

4.4.1 Line Profile Analysis

Instead of using a delta function, thermal X-ray APED model and simple Gaussian function are fitted on the emission spectrum of Capella. Four bright emission lines – Mg XII (λ 8.421), Fe XVII (λ 15.014), O VIII (λ 18.9), and N VII (λ 24.78) – are selected for testing. Upon fitting the parameter for line width dv (converted to velocity scale in km s^{-1}) is allowed to vary. Ideally the parameter dv should be $\approx$ 0 km s^{-1} for thermal APED modeling; however, for Gaussian fitting, the value dv is expected to be ge 0 km s^{-1} as most of these lines are either H-like doublet lines or blended with other weak atomic lines. The results of fitting with the APED model is tabulated in Tables 4 and 5; likewise, the results with the Gaussian model in Tables 6 and 7. Corresponding figures for line profile fit are shown in Figures 3 and 4 for the APED model and in Figures 5 and 6 for the Gaussian model . These are, once again, not meant to be the best fitting parameters.

Upon inspection of Tables 4 through 5, it is noted that the measured line widths are consistent with 0 km s^{-1} for the most of lines. Several measured lines in the outer chips show non-zero widths, although the width is well below the resolution limit ($\sim$ 0.05Å) of LETG.

The same practice with the Gaussian model is repeated and their results show all positive measured line widths, which is expected from blended lines. Note that these four lines are both (1) thermally broadened and (2) broadened due to line blend (e.g., H-like lines are all doublet lines with line separation of 0.005Å). Taking these points into accounts, the expected line widths from Gaussian fitting are 196, 38, 96 and 77 km s^{-1} for Mg XII, Fe XVII, O VIII, and N VII lines. These expected values are, as shown in Tables 6 and 7, fairly close to the observed values.[2]

Figures 3 – 6 show the results of line profile fitting. While the strongest line, Fe XVII λ 15.014, shows some significant residuals in all the line models (aside from the neighboring blended lines not being fit), other line profile models have resulted in a reasonably good fit. While there may be a room for improvement (per insight provided through the Calibration group), these new LSFPARM products can provide fair description of the observed line profiles.

4.4.2 Encircled Energy Fraction

Lastly the model EEFRAC values need to be compared with the observed ones. Here we first compute the theoretical EEFRAC values at three different aperture widths based on the new LSFPARM products. Then at the same aperture widths extract events from an observed dataset. The same Capella dataset (ObsID 55) is chosen for this exercise. Since absolute spectral energy distributions of the target is not known, the ratio

[2] This implies that LETG spectra are aware of these H-like lines being doublet, though these lines are not resolved.

of two entities are compared instead. In this exercise, the ratio of the observed spectra "Extraction B" (at a width equivalent to EEFRAC = 60% at E = 1.497keV) to "Extraction A" (similarly at EEFRAC = 89%, still much narrower than CIAO default extraction width) is compared with the theoretical counterpart. The same exercise is repeated for "Extraction C" (at EEFRAC = 80%) as well. If the EEFRAC values in the LSFPARM products are derived properly, the ratio (as a function of wavelength) should be consistent to each other.

Figure 7 shows the plots of the observed and theoretical ratios of EEFRAC at three extraction widths (A, B, and C). The top two plots show the ratio of Extraction B to A. Notice that *the observed ratio (solid) does not agree with the theoretical ones*, which reveals an unresolved calibration issue. Since the discrepancy between observation and theory is appreciably large, an investigation has been conducted on the difference between MARX and the real dataset. As it turns out, observed cross-dispersion profile in LETG has this excess in the wing part of the profile that is not included into MARX. Figure 8 illustrates the excessive wing structure. The amount of flux found in the excess is about 7% of a total theoretical encircled energy fraction at a wavelength throughout its coverage. Furthermore, the theoretical encircled energy fraction at the core may be overestimated by $\sim 3\%$ when compared to the observed one. By taking the numbers into account, I can reconcile the difference in the ratio ($\sim$0.05).

The reviewer should note that the MARX simulator is used to build these LSF products; and therefore MARX is generally updated to include all the essential information on Chandra instrument, as the information becomes available via the Chandra calibration group. Note that this particular problem on the excess wing has not been characterized and hence is not included in MARX, and hence *is not included in any prior LETG/LSF calibration products in CALDB* that are in use today. So the new LSFPARM products tested here – though admittedly not perfect – still provide *improvement* to the existing LETG+ACIS-S product in CALDB.

To emphasize the point, see the bottom two plots in Figure 7. These plots are the same ratio plots, though with narrower extraction widths B (width $\sim \pm$ 0.0001deg) and C ($\sim \pm$ 0.0002). Since these narrow extraction widths are less susceptible to the excess wing problem, the discrepancy between the observed and theoretical ratios is basically negligible. This indicates that the user may choose to extract his or her LETG-ACIS-S spectra with a "narrower than default" extraction width to minimize this systemic error in flux measurement.

5 Summary

All the testings show that the quality of these new LSFPARM products for unrandomized datasets are as good as one can make based on the available calibration information of LETG and ACIS-S instruments. While some anomalous differences are found in the EEFRAC analysis, this new LSFPARM products will bring in vast improvement on the accuracy in LSF profiles and users' ability to analyze their LETG+ACIS-S datasets.

It goes without saying that, upon availability of new insight on the encircled energy fraction of LETG instrument and incorporation of the new information into MARX, this whole LSFPARM building process will be repeated to improve the quality of LSFPARM products even further.

Table 2. LEG +1st: the Data-to-Model flux ratio

Energy (eV)	Widths (radian)		
	2.84e-4	4.19e-3	1.41e-2
200	1.01	1.01	1.01
275	1.00	1.00	1.00
450	1.00	1.01	1.01
600	1.00	1.00	1.00
800	1.01	1.01	1.01
900	1.01	1.01	1.01
1100	1.01	1.00	1.00
1400	1.00	1.00	1.01
1500	1.00	1.00	1.00
2000	1.01	1.01	1.01
4000	1.01	1.02	1.02
6000	1.01	1.01	1.01

Table 3. LEG -1st: the Data-to-Model flux ratio

Energy (eV)	Widths (radian)		
	2.84e-4	4.19e-3	1.41e-2
200	1.01	1.01	1.01
275	1.01	1.01	1.01
450	1.01	1.01	1.01
600	1.00	1.00	1.00
800	1.01	1.01	1.01
900	1.00	1.00	1.00
1100	1.01	1.01	1.01
1400	1.00	1.00	1.00
1500	1.01	1.01	1.01
2000	1.01	1.00	1.00
4000	1.01	1.01	1.01
6000	1.02	1.01	1.01

Table 4. Capella LEG +1st: thermal APED model.

Element	λ_{lab} (Å)	dv (km/s)	dv 3σ range	χ^2	Comment
Mg XII	8.4192	78.8	0 – 384	2.18	H-like doublet lines
Fe XVII	15.014	0.366	0 – 187	6.43	Seems blended with an unidentified line
O VIII	18.90	139	17.9 – 187	3.70	H-like doublet lines
N VII	24.78	31.5	0 – 216	1.31	Extended line emission?

Table 5. Capella LEG -1st: thermal APED model.

Element	λ_{lab} (Å)	dv (km/s)	dv 3σ range	χ^2	Comment
Mg XII	8.4192	72.6	0 – 270	1.59	H-like doublet lines
Fe XVII	15.014	193	97.7 – 248	3.42	Seems blended with an unidentified line
O VIII	18.90	104	0 – 204	1.59	H-like doublet lines
N VII	24.78	72.6	0 – 270	1.24	Extended line emission?

Table 6. Capella LEG +1st: Simple Gaussian model.

Element	λ_{lab} (Å)	dv (km/s)	dv 3σ range	χ^2	Comment
Mg XII	8.4192	165	0 – 378	1.11	H-like doublet lines
Fe XVII	15.014	25.4	2.50 – 109	9.44	Seems blended with an unidentified line
O VIII	18.90	121	84.7 – 158	2.29	H-like doublet lines
N VII	24.78	70.5	0 – 180	1.33	Extended line emission?

Table 7. Capella LEG -1st: Simple Gaussian model.

Element	λ_{lab} (Å)	dv (km/s)	dv 3σ range	χ^2	Comment
Mg XII	8.4192	209	0 – 420	1.20	H-like doublet lines
Fe XVII	15.014	92.6	0 – 159	4.18	Seems blended with an unidentified line
O VIII	18.90	119	60.6 – 172	1.57	H-like doublet lines
N VII	24.78	74.3	0 – 224	1.38	Extended line emission?

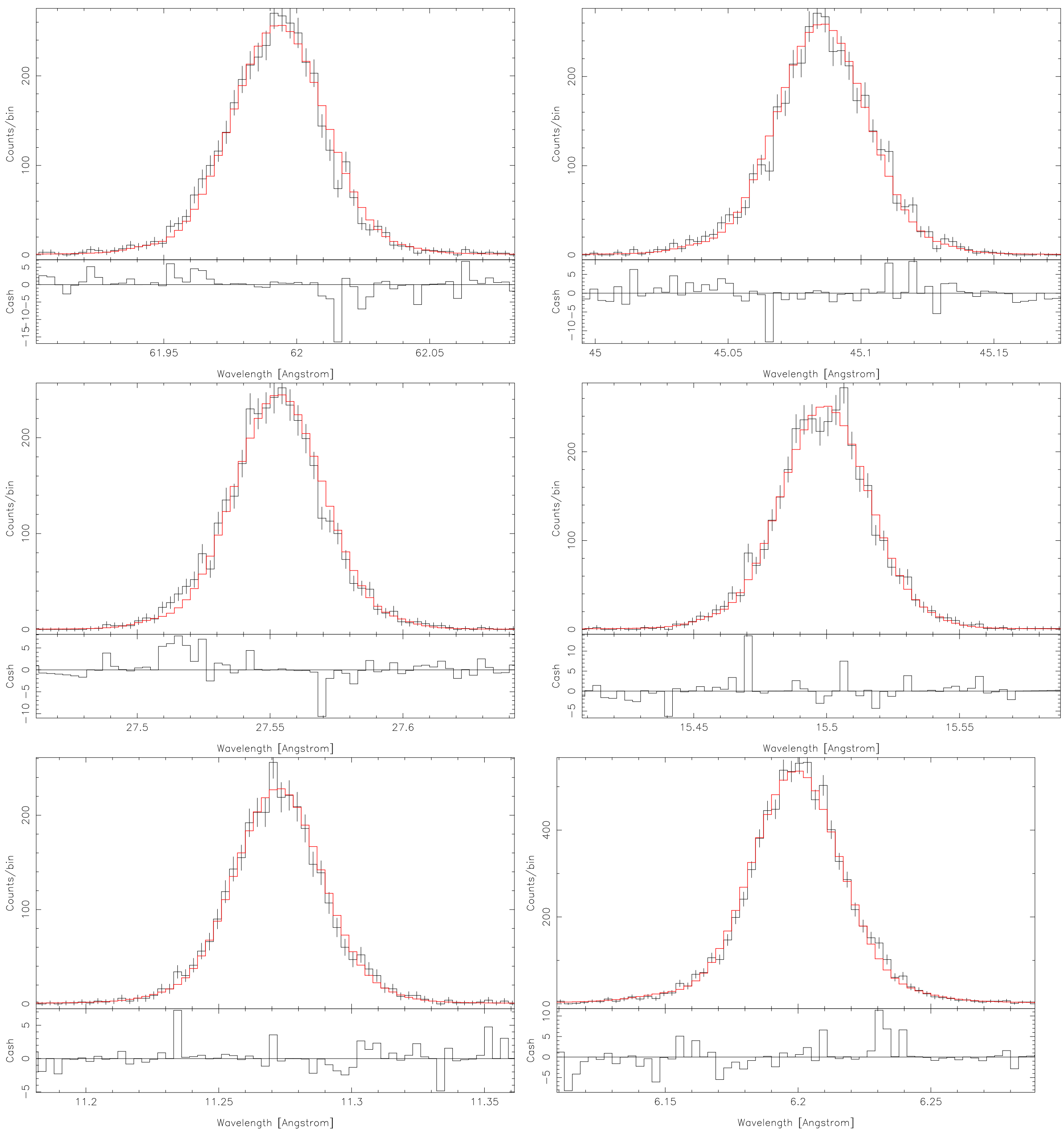

Figure 1: LEG +1st-order line profiles, fitted with a Kronecker delta function (red) folded over LEG +1st order grating RMFs: (top right) line profile at E = 200 eV, with a goodness of fit χ^2 = 1.80; (top left) E = 275 eV, χ^2 = 1.85; (middle left) E = 450 eV, χ^2 = 1.61; (middle right) E = 800 eV, χ^2 = 1.29; (bottom right) E = 1100 eV,χ^2 =1.01; and (bottom left) E = 2000 eV, χ^2 = 1.71. The delta function model describes simulated line profiles fairly well.

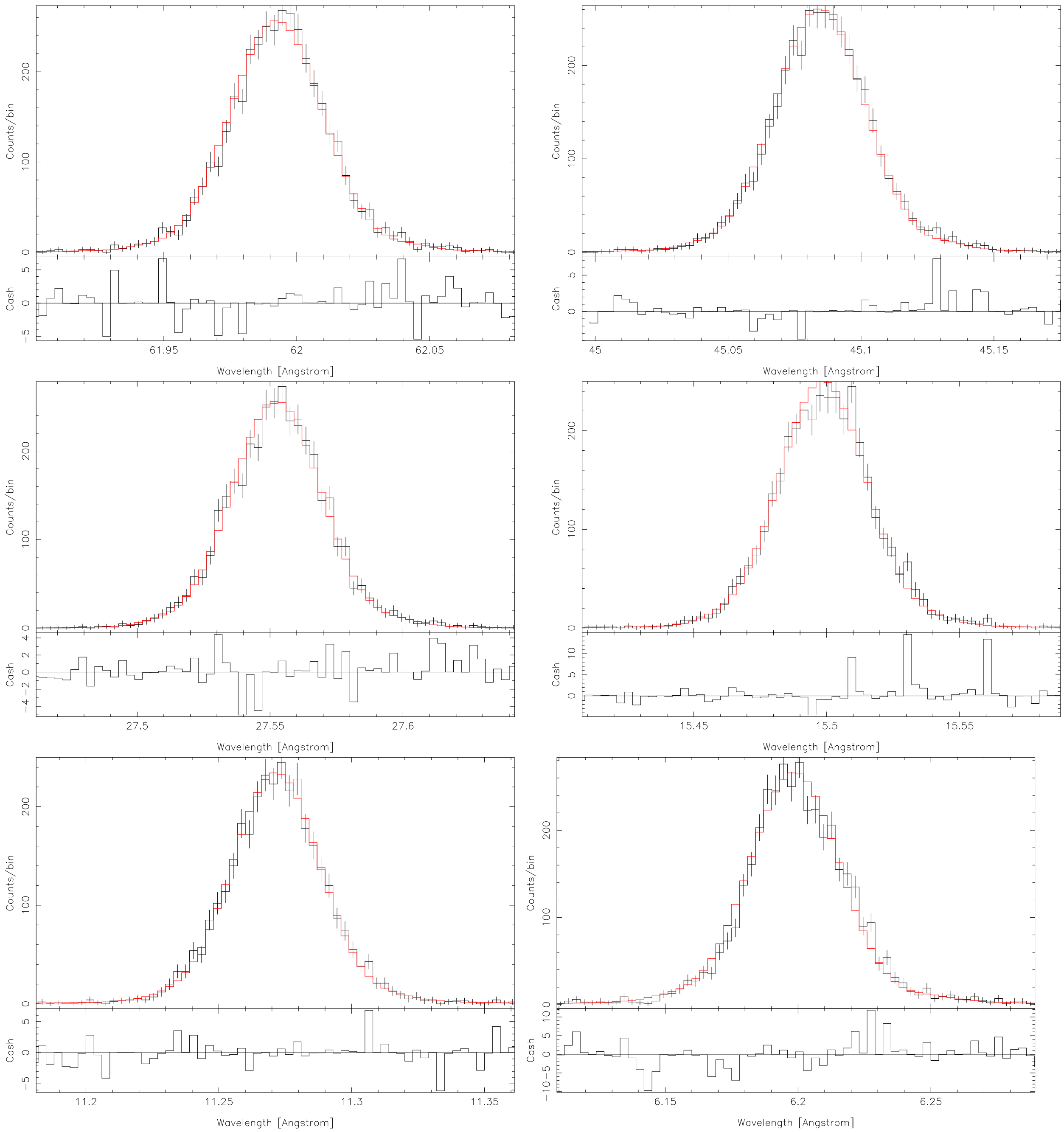

Figure 2: LEG +1st-order line profiles: (top right) line profile at E = 200 eV, with a goodness of fit χ^2 = 1.41; (top left) E = 275 eV, χ^2 = 0.818; (middle left) E = 450 eV, χ^2 = 1.11; (middle right) E = 800 eV, χ^2 = 1.35; (bottom right) E = 1100 eV,χ^2 =1.09; and (bottom left) E = 2000 eV, χ^2 = 2.10.

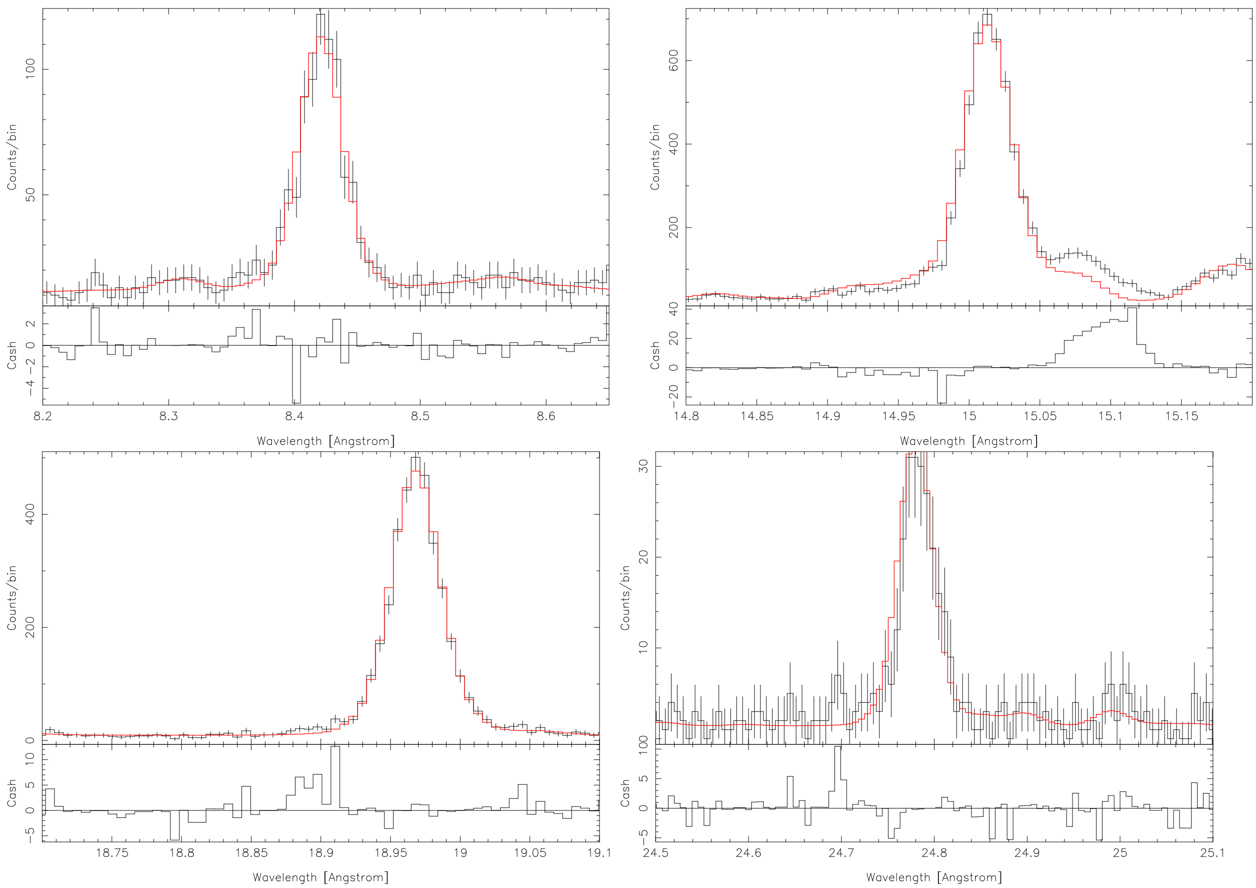

Figure 3: Selected LEG +1st-order Capella line profiles; (top left) Mg XII line, fitted with an APED thermal model (red) and its goodness of fit $\chi^2 = 1.00$; (top right) Fe XVII with $\chi^2 = 6.43$; (bottom left) O VIII with $\chi^2 = 3.70$; (bottom right) N VII with $\chi^2 = 1.31$. This simplified APED model (not necessarily the best fit) adequately describes the Capella line spectra, though the atomic model may be lacking in its accuracy, which lead to higher χ^2 values.

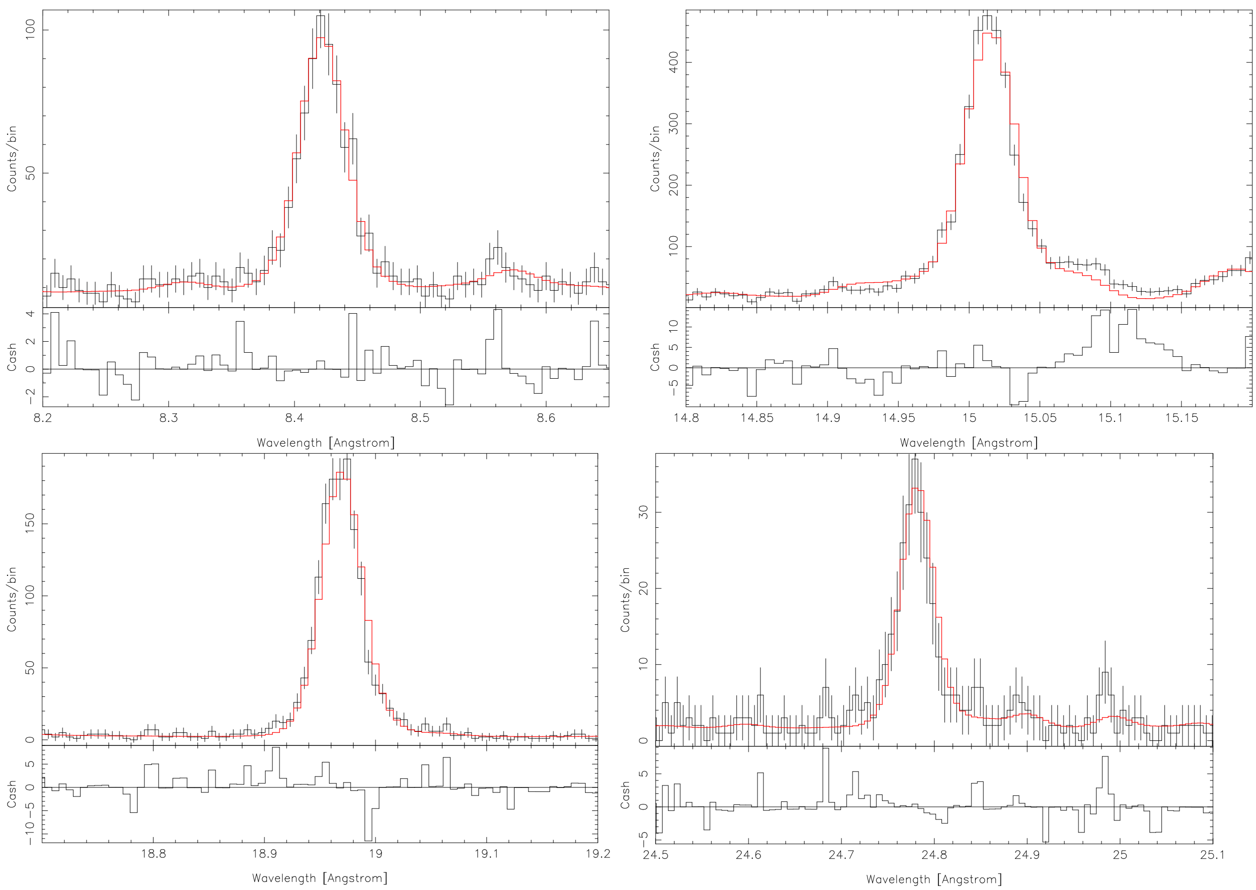

Figure 4: Selected LEG -1st-order Capella line profiles; (top left) Mg XII line, fitted with an APED thermal model (red) and its goodness of fit $\chi^2 = 0.902$; (top right) Fe XVII with $\chi^2 = 3.42$; (bottom left) O VIII with $\chi^2 = 1.59$; (bottom right) N VII with $\chi^2 = 1.24$.

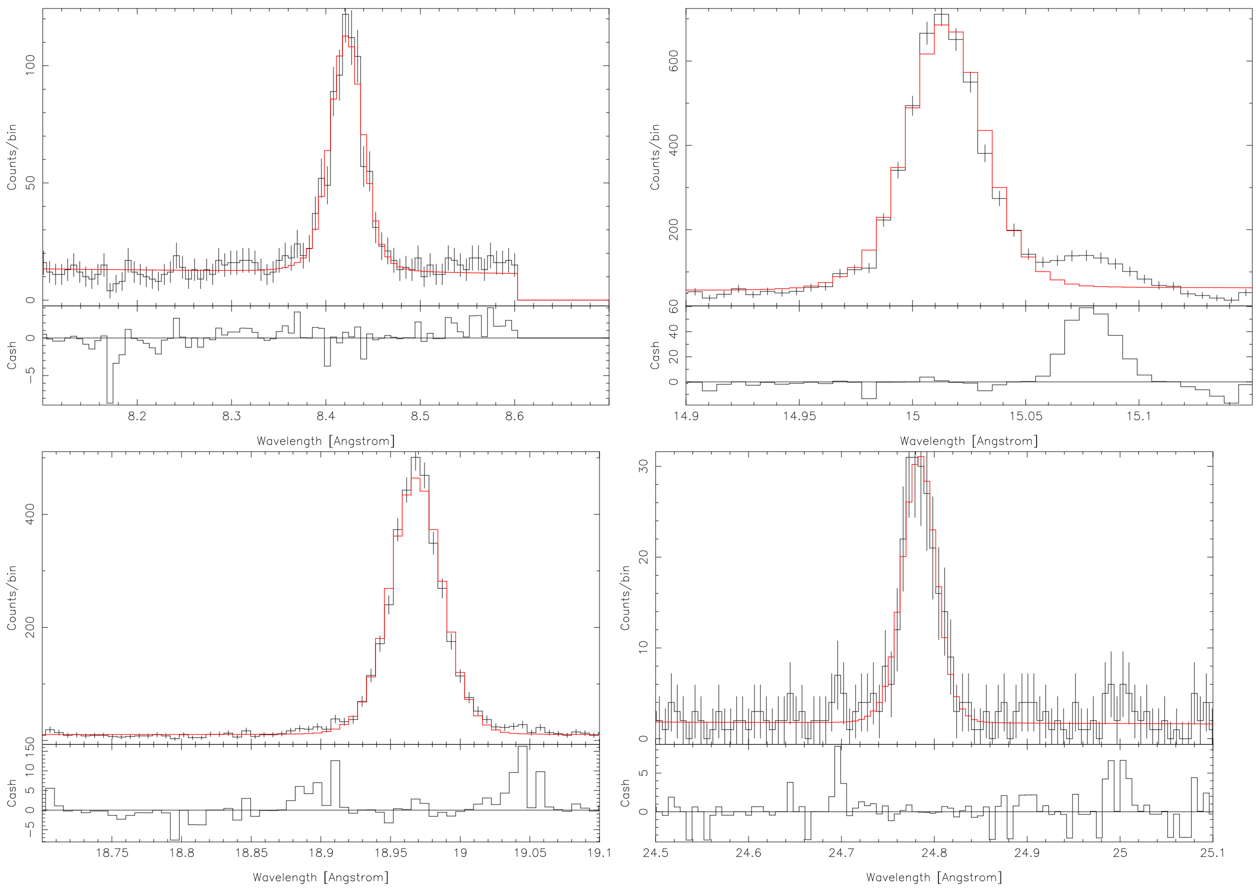

Figure 5: Selected LEG +1st-order Capella line profiles; (top left) Mg XII line, fitted with a single Gaussian function (red; velocity width $dv \approx 165\text{km s}^{-1}$) and its goodness of fit $\chi^2 = 1.11$;(top right) Fe XVII ($dv \approx 25.4\text{km s}^{-1}$) with $\chi^2 = 9.44$; (bottom left) O VIII ($dv \approx 121\text{km s}^{-1}$) with $\chi^2 = 2.29$; (bottom right) N VII ($dv \approx 70.5\text{km s}^{-1}$) with $\chi^2 = 1.33$.

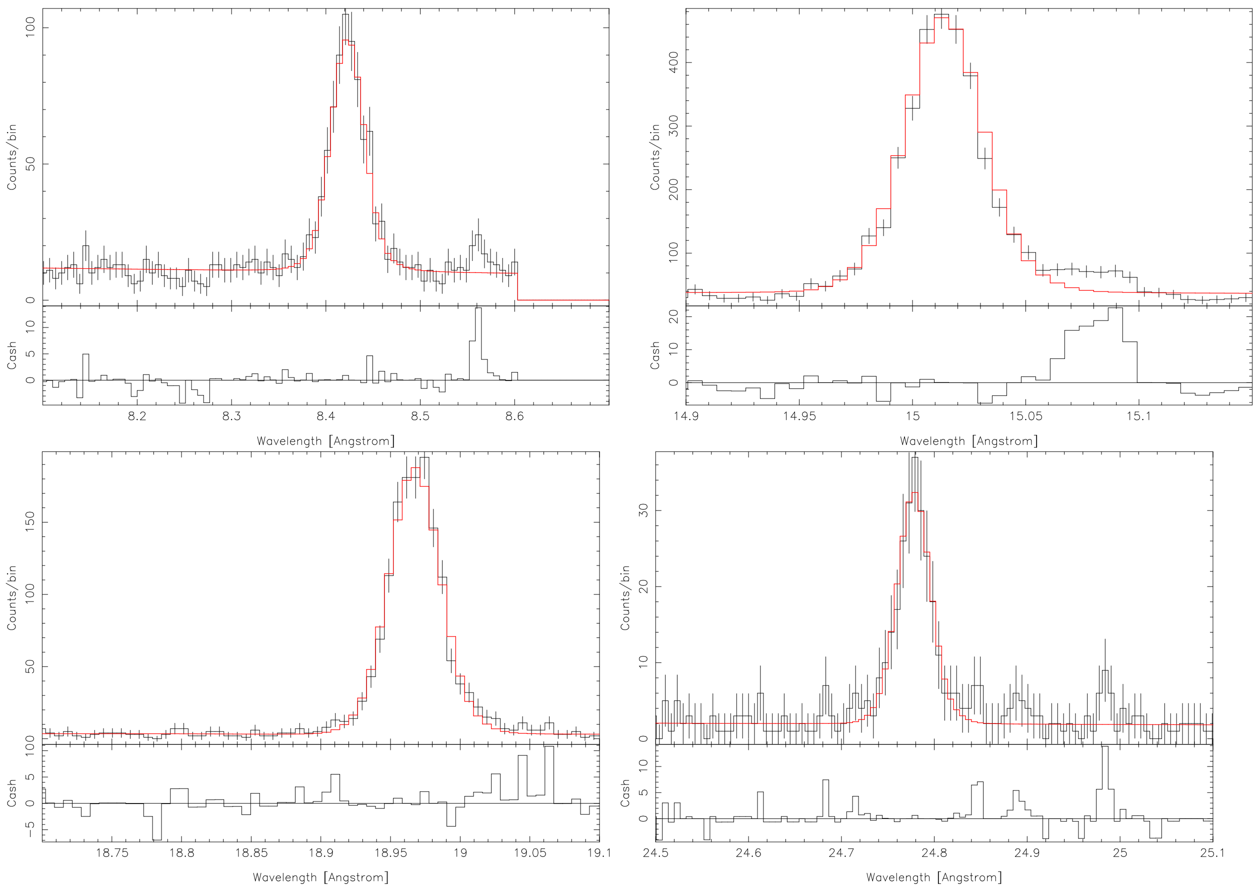

Figure 6: Selected LEG -1st-order Capella line profiles; (top left) Mg XII line, fitted with a single Gaussian function (red; velocity width $dv \approx 209$km s^{-1}) and its goodness of fit $\chi^2 = 1.20$;(top right) Fe XVII ($dv \approx 92.6$km s^{-1}) with $\chi^2 = 4.18$; (bottom left) O VIII ($dv \approx 119$km s^{-1}) with $\chi^2 = 1.57$; (bottom right) N VII ($dv \approx 74.3$km s^{-1}) with $\chi^2 = 1.38$.

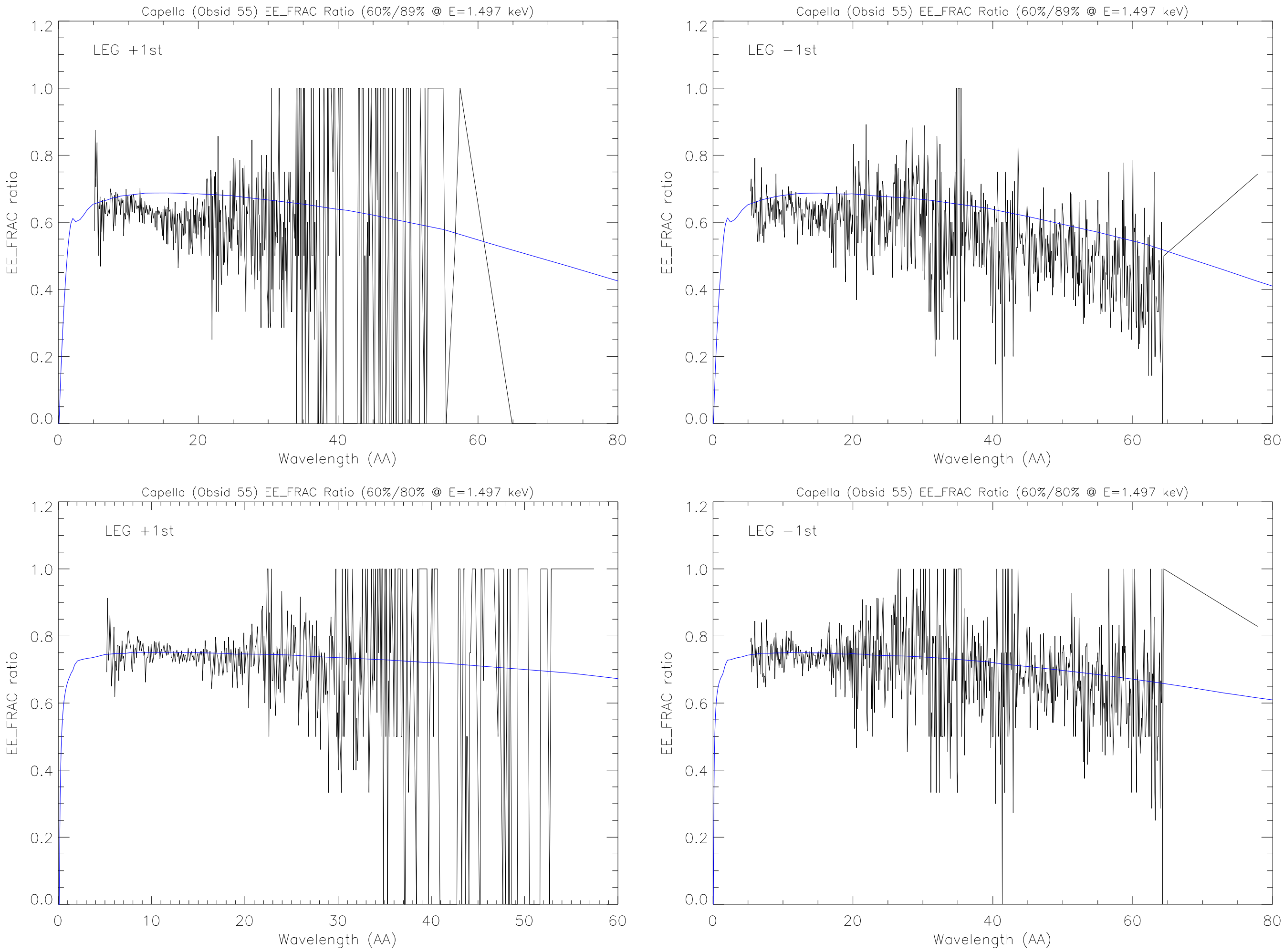

Figure 7: Ratio plots of theoretical (blue) and Capella's observed (black) EEFRAC values: (top left) LEG +1st, the ratio of Extraction B to A; (top right) LEG -1st, the ratio of Extraction B to A; (bottom left) LEG +1st, the ratio of Extraction B to C; (bottom right) LEG -1st, the ratio of Extraction B to C.

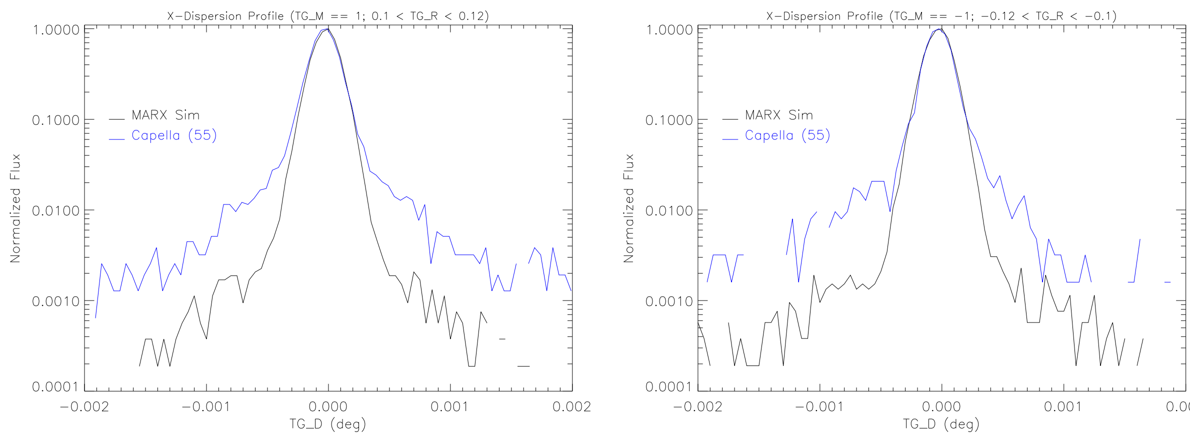

Figure 8: Uncalibrated cross-dispersion feature in LETG (left LEG +1st; right LEG -1st). The solid line shows the MARX model of LETG spectra projected onto ACIS-S; the blue line shows the observed LETG spectra of Capella. The excess in the wing of cross-dispersion profile is relatively weak and presumably not detected by the LETG calibration group. The magnitude of the excess is not likely to be detected with HRC-S since the detector noise level is much higher.